Permanent Magnet Wind Generator Technology for Battery Charging Wind Energy Systems

Casper J. J. Labuschagne, Maarten J. Kamper

Electrical Machines Laboratory
Dept of Electrical and Electronic Engineering
Stellenbosch University

September 2018

Outline

Introduction

Active Battery Charging System

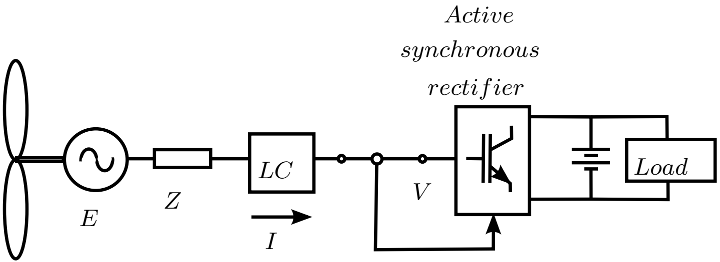

Figure 1: Single line diagram of PM wind generator connected to active battery charging system with actively synchronous rectifier.

Passive Battery Charging System

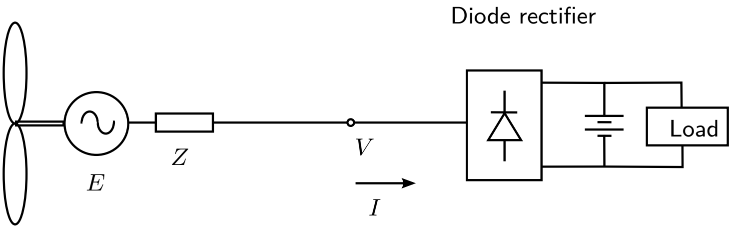

Figure 2: Single line diagram of PM wind generator connected to passive battery charging system with uncontrolled diode rectifier.

PMSG

- Permanent magnet synchronous generator
- Direct-drive
- Low cogging torque
- Relatively large internal synchronous inductance

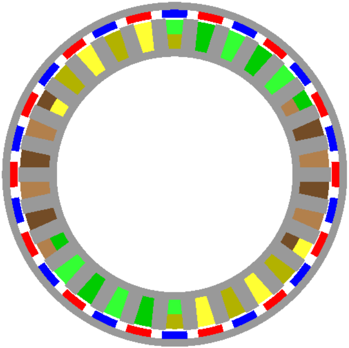

Figure 3: Cross section of the radial flux outer rotor PMSG configuration with surface mounted PMs

Passive Battery Charging System

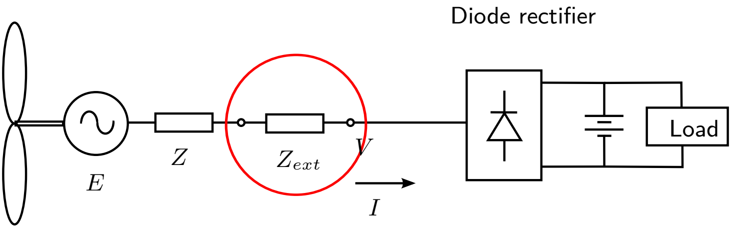

Figure 4: Single line diagram of PM wind generator connected to passive battery charging system with uncontrolled diode rectifier.

Passive Battery Charging System

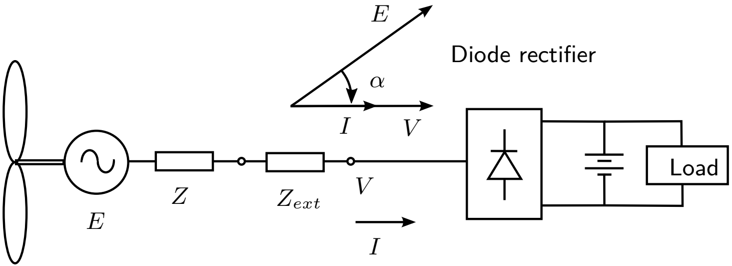

Figure 5: Single line diagram of PM wind generator connected to passive battery charging system with uncontrolled diode rectifier.

Static FEA method is proposed to achieve maximum power point matching for a turbine-specific design using an external inductance.

Active Battery Charging System

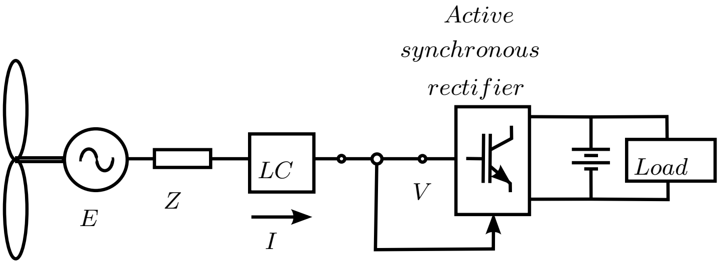

Figure 6: Single line diagram of PM wind generator connected to active battery charging system with actively synchronous rectifier.

Wind Turbine Battery Charging System

Power Matching

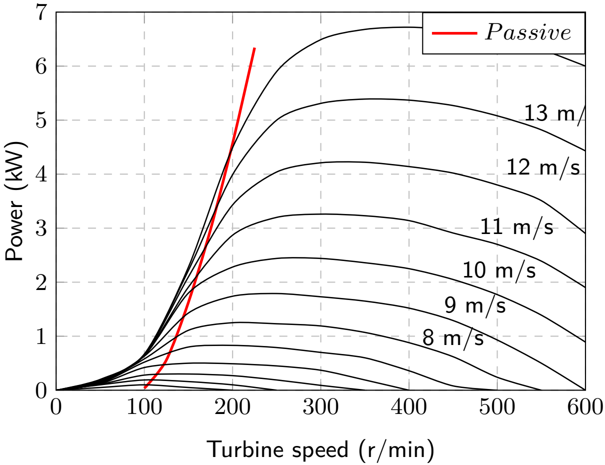

Figure 7: Wind turbine power versus turbine speed curves with wind speed a parameter, and operating power curves for passive and active systems.

Power Matching

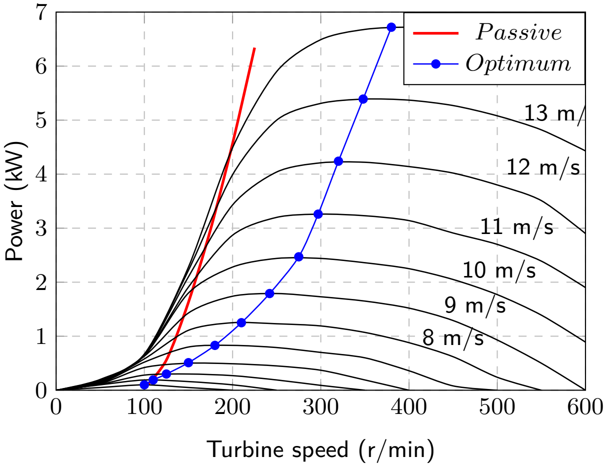

Figure 7: Wind turbine power versus turbine speed curves with wind speed a parameter, and operating power curves for passive and active systems.

Power Matching

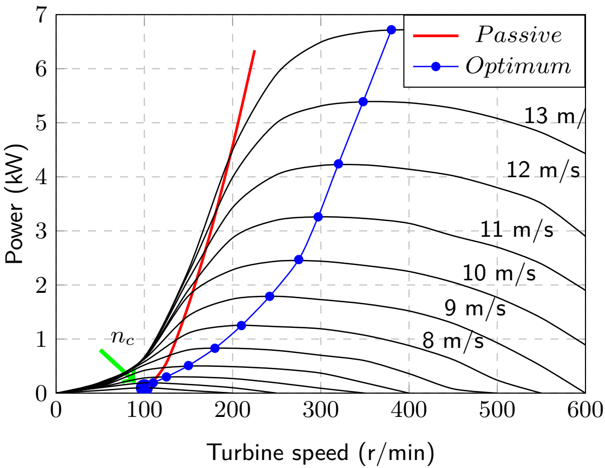

Figure 7: Wind turbine power versus turbine speed curves with wind speed a parameter, and operating power curves for passive and active systems.

Power Matching

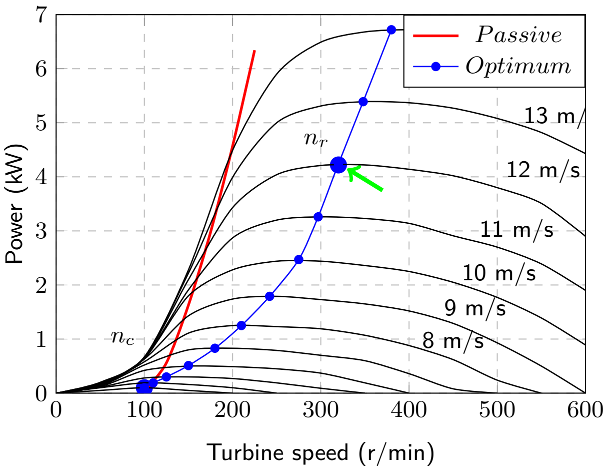

Figure 7: Wind turbine power versus turbine speed curves with wind speed a parameter, and operating power curves for passive and active systems.

System Requirements

Table 1: Wind generator operating points for passive battery charging system

	n_c	n_r
Wind speed	3 m/s	12 m/s
Turbine speed	100 r/min	320 r/min
Power	0 kW	4.2 kW

Steady-State FE Simulation Method

Steady-State FE Simulation Method

- State of the PMSG? ($\alpha = \Delta$)
- External Inductance L_{ext}?

Static FEA Iterations

1^{st} Iteration

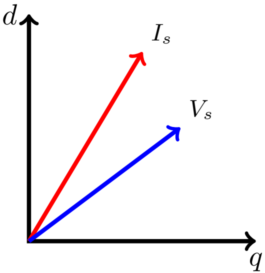

$(\alpha \neq \Delta)$

Static FEA Iterations

1^{st} Iteration

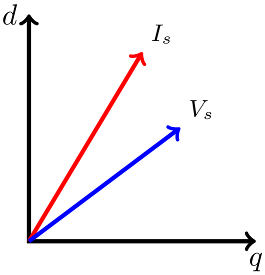

$(\alpha \neq \Delta)$

2^{nd} Iteration

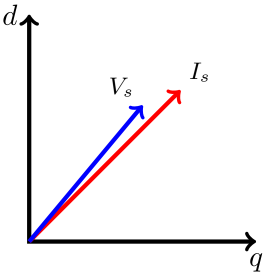

$(\alpha \neq \Delta)$

Static FEA Iterations

1^{st} Iteration

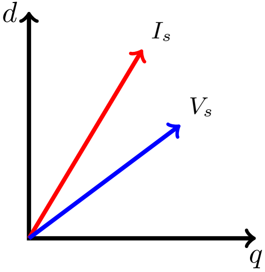

$(\alpha \neq \Delta)$

2^{nd} Iteration

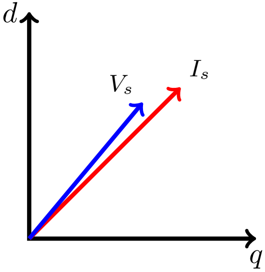

$(\alpha \neq \Delta)$

3^{rd} Iteration

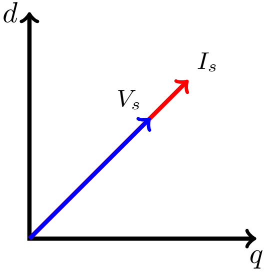

$(\alpha \approx \Delta)$

External Inductance Calculation

External Inductance L_{ext}

$$L_{ext} = L_1 \qquad L_{ext} = L_2 \qquad L_{ext} = L_3$$

External Inductance Calculation

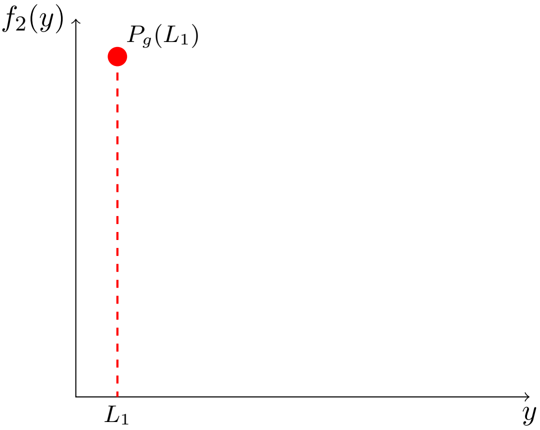

Figure 8: Second degree polynomial obtained from curve fitting of the static FEA solutions, and calculating L_{ext} from the rated power P_g.

External Inductance Calculation

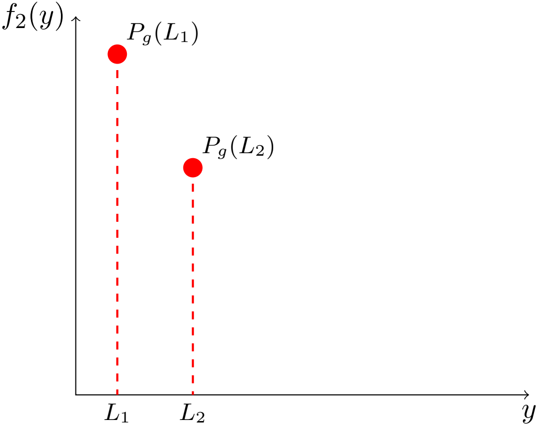

Figure 8: Second degree polynomial obtained from curve fitting of the static FEA solutions, and calculating L_{ext} from the rated power P_g.

External Inductance Calculation

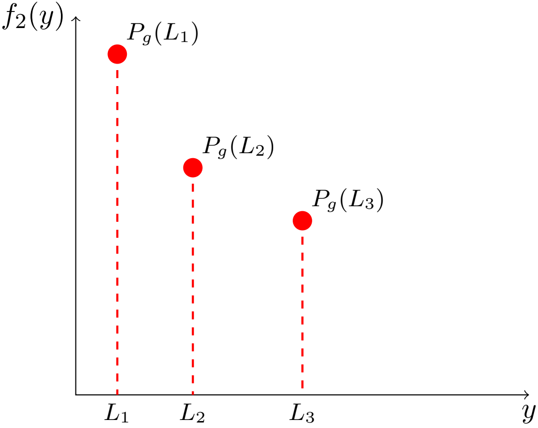

Figure 8: Second degree polynomial obtained from curve fitting of the static FEA solutions, and calculating L_{ext} from the rated power P_g.

External Inductance Calculation

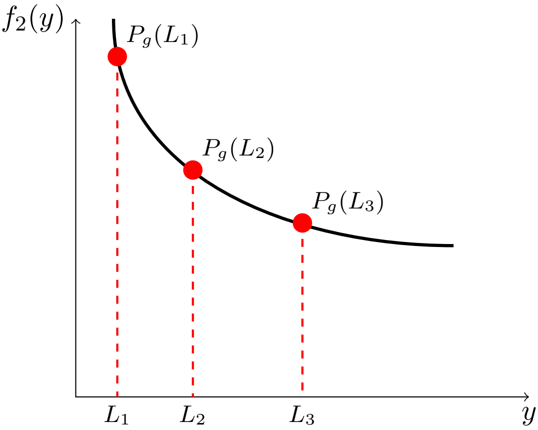

Figure 8: Second degree polynomial obtained from curve fitting of the static FEA solutions, and calculating L_{ext} from the rated power P_g.

External Inductance Calculation

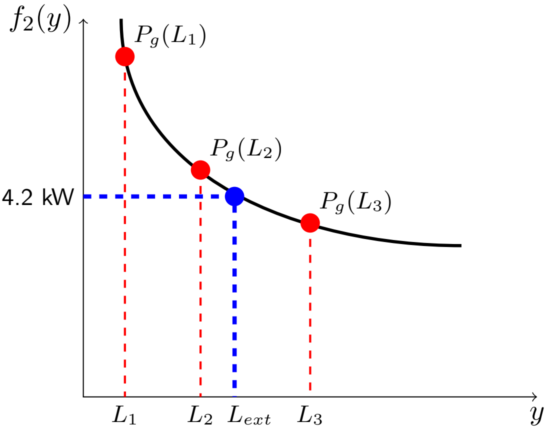

Figure 8: Second degree polynomial obtained from curve fitting of the static FEA solutions, and calculating L_{ext} from the rated power P_g.

Static FEA method

- Design for cut-in point. (1)
- Solve for $L_{ext} = L_1$. (3)
- Solve for $L_{ext} = L_2$. (3)
- Solve for $L_{ext} = L_3$. (3)
- Determine actual L_{ext}.
- Solve PMSG. (3)
- Evaluate final performance.

Optimisation

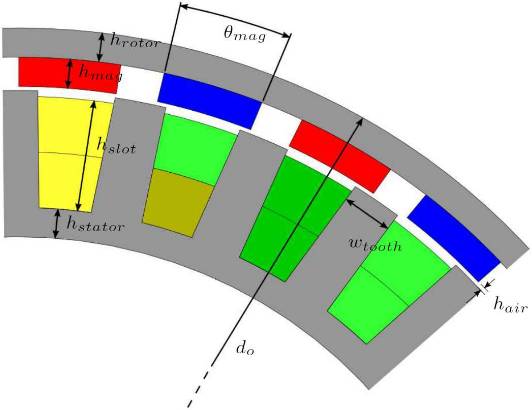

Figure 9: Cross section of the double layer non-overlap winding PMSG indicating the relevant dimensions for design and optimisation.

$$\mathbf{X} = \begin{bmatrix} d_o \\ h_{rotor} \\ h_{mag} \\ \theta_{mag} \\ h_{slot} \\ w_{tooth} \\ h_{stator} \\ l \end{bmatrix} \quad (1)$$

Non-dominated Sorting Genetic Algorithm II

Performance constraints

$$\mathbf{U} = \begin{bmatrix} P_{gen} \\ \eta \\ J \end{bmatrix} = \begin{bmatrix} 4.2kW \\ \geq 90\% \\ \leq 6A/mm^2 \end{bmatrix}$$

Objective function

$$minimise\ \mathbf{F}(\mathbf{X}) = \begin{bmatrix} M_{active}(\mathbf{X}) \\ M_{PM}(\mathbf{X}) \end{bmatrix}$$

Simulation Results

Simulation Results

- Effect of L_{ext} on power point matching
- Effect of number of poles
- Effect of generator size
- Static FEA performance

Effect of L_{ext} on Power Point Matching

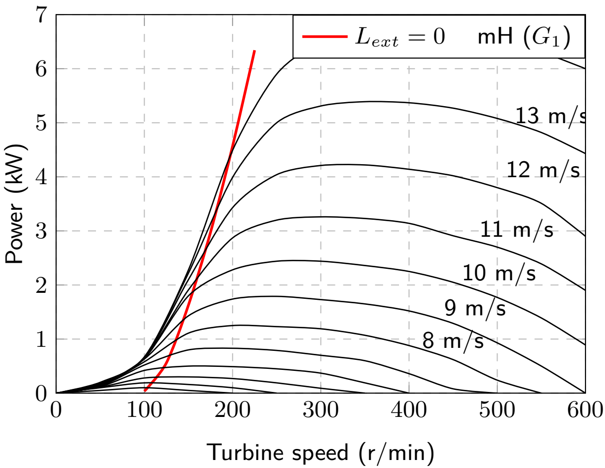

Figure 10: Power matching of the 28/30 wind generator (G_1 and G_1^*) with L_{ext} a parameter.

Effect of L_{ext} on Power Point Matching

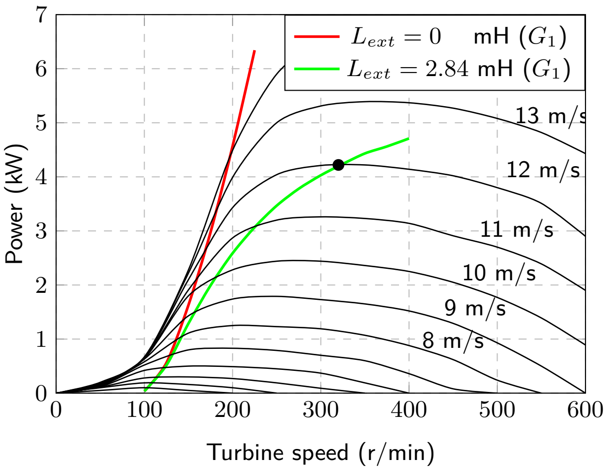

Figure 10: Power matching of the 28/30 wind generator (G_1 and G_1^*) with L_{ext} a parameter.

Effect of L_{ext} on Power Point Matching

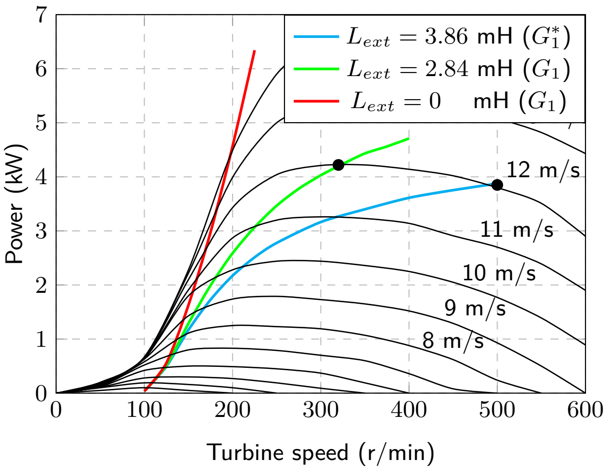

Figure 10: Power matching of the 28/30 wind generator (G_1 and G_1^*) with L_{ext} a parameter.

Table 2: Static FEA results for $28/30$ pole PMSG.

	G_1	G_2	G_1^*
P_g, kW	4.22	4.25	3.86
f_s, Hz	74.67	74.67	116.67
$Turns\ per\ winding,\ N_s$	14	10	14
V_{rms}	23.5	23.6	23.65
J, A/mm^2	4.67	3.29	4.37
α	54.4°	54.4°	68.8°
η, %	90.4	92.4	88.6
X_s, p.u.	0.58	0.46	0.83
X_{ext}, p.u.	1.88	1.99	3.59
L_{ext}, mH	2.84	3.06	3.74
X_{ext}/X_s	3.26	4.33	4.32
$Outer\ Diameter$, mm	384	384	384
$Axial\ Length$, mm	70.55	100	70.55
M_{active}	22.08	32.1	22.7
M_{PM}	2.77	3.72	2.63

Optimisation Results

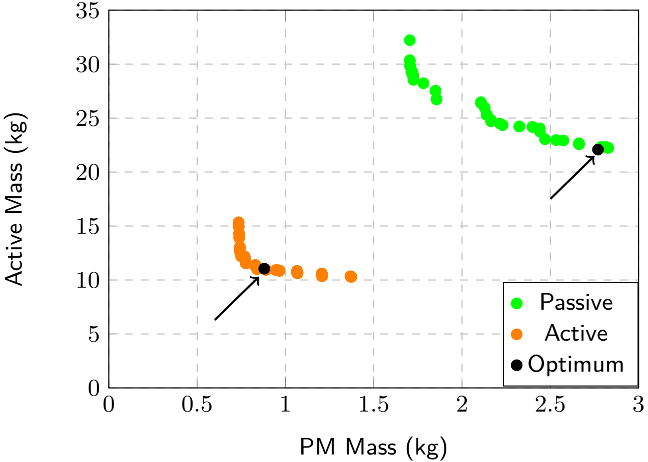

Figure 11: Pareto fronts of PM mass versus active mass of the PMSGs for the passive and acive systems, with the chosen optimal design points indicated.

Table 3: Design optimisation results and component ratios

Parameters	Passive	Active	Pas:Act
Outer diameter, d_o (mm)	384	350	1:0.91
Stator height, h_{rotor} (mm)	6.8	4.74	1:0.70
Magnet height, h_{mag} (mm)	6.2	3	1:0.48
Magnet pitch, θ_{mag} (%)	0.7	0.7	1:1
Slot height, h_{slot} (mm)	35.1	31.6	1:0.90
Tooth width, w_{tooth} (mm)	12	8	1:0.67
Rotor height, h_{stator} (mm)	5.8	4.125	1:0.71
Axial length, l (mm)	70.55	50	1:0.71
Active iron mass (kg)	14.24	6.41	1:0.45
Copper mass (kg)	5.07	3.76	1:0.74
PM mass (kg)	2.77	0.88	1:0.32
Total active mass (kg)	22.08	11.05	1:0.50
External reactance, X_{ext} (p.u.)	1.88	-	
Current density, (A/mm^2)	4.67	6.0	
Current angle, α (degrees)	54.4	0	
Rated power, P_g (kW)	4.22	4.26	
Efficiency, η (%)	90.4	90	

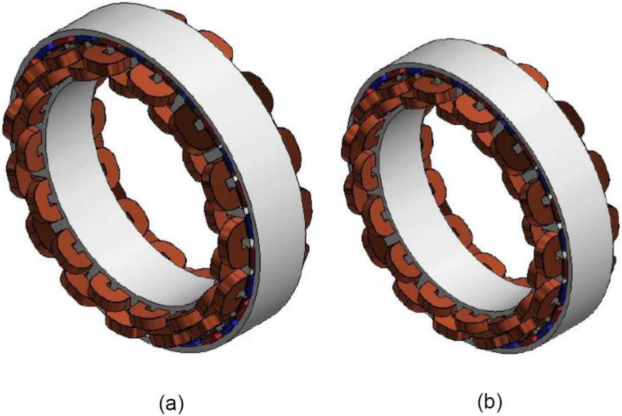

Figure 12: To scale representation of the optimised PMSGs in Table 3 for (a) passive and (b) active systems.

Conclusions

Conclusions

Static FE Simulation Method

- Passive charging systems have poor power matching with no external inductance.
- The proposed method is accurate and not computationally expensive.
- For maximum power point matching using non-overlap winding machines, X_{ext}/X_s is about a factor 4.
- Higher frequency generators require a much reduced external inductance, although slightly less efficiency.
- The proposed calculation method can be used excellently to do a wind site specific design optimization of the system, maximizing annual wind energy harvesting and minimizing generator and external inductance sizes.

Conclusions

Optimal Design

- The passive system's generator active mass is almost twice that of the active system's generator active mass.
- The active system generator also outperforms the passive system generator in terms of PM mass, where it is found that the active system generator's PM mass is three times less.
- The passive system PMSG is more expensive to manufacture and the wind tower structure will most likely also be more expensive. Also requires large L_{ext}.
- The active system requires an LC filter and an expensive rectifier with complex position-sensorless control.

Thank you.

Contact: Casper Labuschagne
E-mail: 17539455@sun.ac.za

Effect of Number of Poles

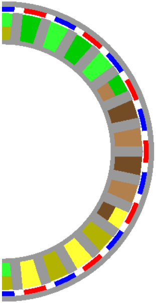

(a)

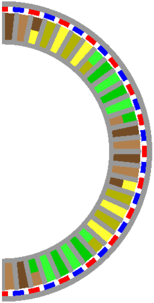

(b)

Figure 13: Different pole-slot configurations for PMSG where (a) 28/30 pole-slot combination and (b) 56/60 pole-slot combination.

Table 4: Static FEA results for $28/30$ pole PMSG and $56/60$ pole PMSGs.

	G_1	G_2	G_1^*	G_3	G_4
P_g, kW	4.22	4.25	3.86	4.20	4.25
f_s, Hz	74.67	74.67	116.67	149.33	149.33
$Turns\ per\ winding,\ N_s$	14	10	14	7	5
V_{rms}	23.5	23.6	23.65	24.0	24.0
J, A/mm^2	4.67	3.29	4.37	4.58	3.15
α	$54.4°$	$54.4°$	$68.8°$	$54.6°$	$54.7°$
η, %	90.4	92.4	88.6	89.62	90.46
X_s, p.u.	0.58	0.46	0.83	0.571	0.449
X_{ext}, p.u.	1.88	1.99	3.59	1.87	1.96
L_{ext}, mH	2.84	3.06	3.74	1.47	1.61
X_{ext}/X_s	3.26	4.33	4.32	3.27	4.37
$Outer\ Diameter$, mm	384	384	384	384	384
$Axial\ Length$, mm	70.55	100	70.55	70.55	100
M_{active}	22.08	32.1	22.7	22.08	32.1
M_{PM}	2.77	3.72	2.63	2.77	3.72

Table 4: Static FEA results for $28/30$ pole PMSG and $56/60$ pole PMSGs.

	G_1	G_2	G_1^*	G_3	G_4
P_g, kW	4.22	4.25	3.86	4.20	4.25
f_s, Hz	74.67	74.67	116.67	149.33	149.33
$Turns\ per\ winding,\ N_s$	14	10	14	7	5
V_{rms}	23.5	23.6	23.65	24.0	24.0
J, A/mm^2	4.67	3.29	4.37	4.58	3.15
α	54.4°	54.4°	68.8°	54.6°	54.7°
η, %	90.4	92.4	88.6	89.62	90.46
X_s, p.u.	0.58	0.46	0.83	0.571	0.449
X_{ext}, p.u.	1.88	1.99	3.59	1.87	1.96
L_{ext}, mH	2.84	3.06	3.74	1.47	1.61
X_{ext}/X_s	3.26	4.33	4.32	3.27	4.37
$Outer\ Diameter$, mm	384	384	384	384	384
$Axial\ Length$, mm	70.55	100	70.55	70.55	100
M_{active}	22.08	32.1	22.7	22.08	32.1
M_{PM}	2.77	3.72	2.63	2.77	3.72

Effect of Generator Size

- Geometric dimensions held constant.
- Axial Length

Table 5: Static FEA results for $28/30$ pole PMSG and $56/60$ pole PMSGs.

	G_1	G_2	G_1^*	G_3	G_4
P_g, kW	4.22	4.25	3.86	4.20	4.25
f_s, Hz	74.67	74.67	116.67	149.33	149.33
$Turns\ per\ winding,\ N_s$	14	10	14	7	5
V_{rms}	23.5	23.6	23.65	24.0	24.0
J, A/mm^2	4.67	3.29	4.37	4.58	3.15
α	$54.4°$	$54.4°$	$68.8°$	$54.6°$	$54.7°$
η, %	90.4	92.4	88.6	89.62	90.46
X_s, p.u.	0.58	0.46	0.83	0.571	0.449
X_{ext}, p.u.	1.88	1.99	3.59	1.87	1.96
L_{ext}, mH	2.84	3.06	3.74	1.47	1.61
X_{ext}/X_s	3.26	4.33	4.32	3.27	4.37
$Outer\ Diameter$, mm	384	384	384	384	384
$Axial\ Length$, mm	70.55	100	70.55	70.55	100
M_{active}	22.08	32.1	22.7	22.08	32.1
M_{PM}	2.77	3.72	2.63	2.77	3.72

Table 5: Static FEA results for $28/30$ pole PMSG and $56/60$ pole PMSGs.

	G_1	G_2	G_1^*	G_3	G_4
P_g, kW	4.22	4.25	3.86	4.20	4.25
f_s, Hz	74.67	74.67	116.67	149.33	149.33
$Turns\ per\ winding,\ N_s$	14	10	14	7	5
V_{rms}	23.5	23.6	23.65	24.0	24.0
J, A/mm^2	4.67	3.29	4.37	4.58	3.15
α	54.4°	54.4°	68.8°	54.6°	54.7°
η, %	90.4	92.4	88.6	89.62	90.46
X_s, p.u.	0.58	0.46	0.83	0.571	0.449
X_{ext}, p.u.	1.88	1.99	3.59	1.87	1.96
L_{ext}, mH	2.84	3.06	3.74	1.47	1.61
X_{ext}/X_s	3.26	4.33	4.32	3.27	4.37
$Outer\ Diameter$, mm	384	384	384	384	384
$Axial\ Length$, mm	70.55	100	70.55	70.55	100
M_{active}	22.08	32.1	22.7	22.08	32.1
M_{PM}	2.77	3.72	2.63	2.77	3.72

Table 5: Static FEA results for $28/30$ pole PMSG and $56/60$ pole PMSGs.

	G_1	G_2	G_1^*	G_3	G_4
P_g, kW	4.22	4.25	3.86	4.20	4.25
f_s, Hz	74.67	74.67	116.67	149.33	149.33
$Turns\ per\ winding,\ N_s$	14	10	14	7	5
V_{rms}	23.5	23.6	23.65	24.0	24.0
J, A/mm^2	4.67	3.29	4.37	4.58	3.15
α	54.4°	54.4°	68.8°	54.6°	54.7°
η, %	90.4	92.4	88.6	89.62	90.46
X_s, p.u.	0.58	0.46	0.83	0.571	0.449
X_{ext}, p.u.	1.88	1.99	3.59	1.87	1.96
L_{ext}, mH	2.84	3.06	3.74	1.47	1.61
X_{ext}/X_s	3.26	4.33	4.32	3.27	4.37
$Outer\ Diameter$, mm	384	384	384	384	384
$Axial\ Length$, mm	70.55	100	70.55	70.55	100
M_{active}	22.08	32.1	22.7	22.08	32.1
M_{PM}	2.77	3.72	2.63	2.77	3.72

Table 5: Static FEA results for $28/30$ pole PMSG and $56/60$ pole PMSGs.

	G_1	G_2	G_1^*	G_3	G_4
P_g, kW	4.22	4.25	3.86	4.20	4.25
f_s, Hz	74.67	74.67	116.67	149.33	149.33
$Turns\ per\ winding,\ N_s$	14	10	14	7	5
V_{rms}	23.5	23.6	23.65	24.0	24.0
J, A/mm^2	4.67	3.29	4.37	4.58	3.15
α	54.4°	54.4°	68.8°	54.6°	54.7°
η, %	90.4	92.4	88.6	89.62	90.46
X_s, p.u.	0.58	0.46	0.83	0.571	0.449
X_{ext}, p.u.	1.88	1.99	3.59	1.87	1.96
L_{ext}, mH	2.84	3.06	3.74	1.47	1.61
X_{ext}/X_s	3.26	4.33	4.32	3.27	4.37
$Outer\ Diameter$, mm	384	384	384	384	384
$Axial\ Length$, mm	70.55	100	70.55	70.55	100
M_{active}	22.08	32.1	22.7	22.08	32.1
M_{PM}	2.77	3.72	2.63	2.77	3.72

Static FEA Performance

Table 6: General performance of the static FEA simulations

	G_1	G_3
Mesh Elements	17731	18241
FEA iterations	13	13
Total simulation time, s	28.8	33.7

Static FEA Performance

Table 6: General performance of the static FEA simulations

	G_1	G_3
Mesh Elements	17731	18241
FEA iterations	13	13
Total simulation time, s	28.8	33.7

Verification

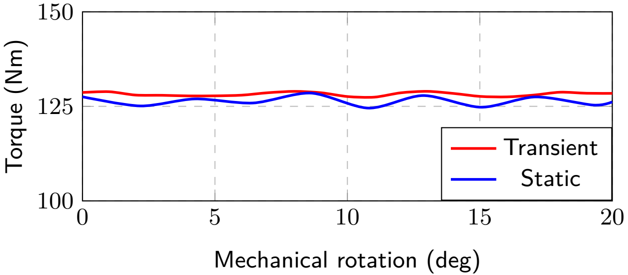

Figure 14: Developed torque versus mechanical rotation obtained from transient (ANSYS Maxwell) and static (SEMFEM) solutions.